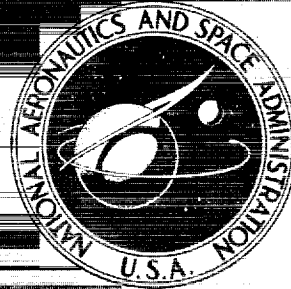


**NASA TECHNICAL
MEMORANDUM**



N73-31828
NASA TM X-2828

NASA TM X-2828

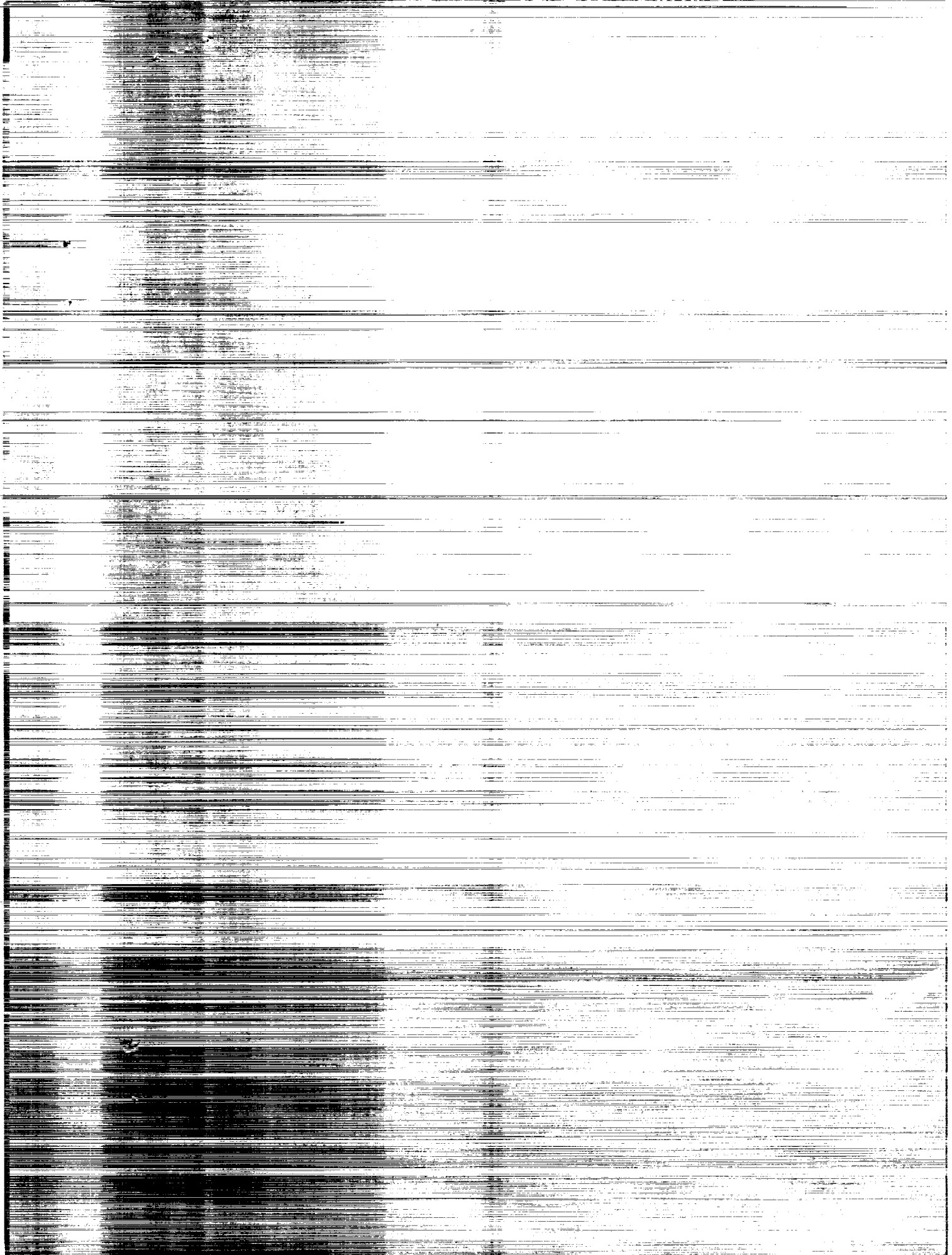
NASA TM X-2828

**CASE FILE
COPY**

**ANALYTICAL AND EXPERIMENTAL STUDY
OF SUPERSONIC COMBUSTION OF
HYDROGEN IN A VITIATED AIRSTREAM**

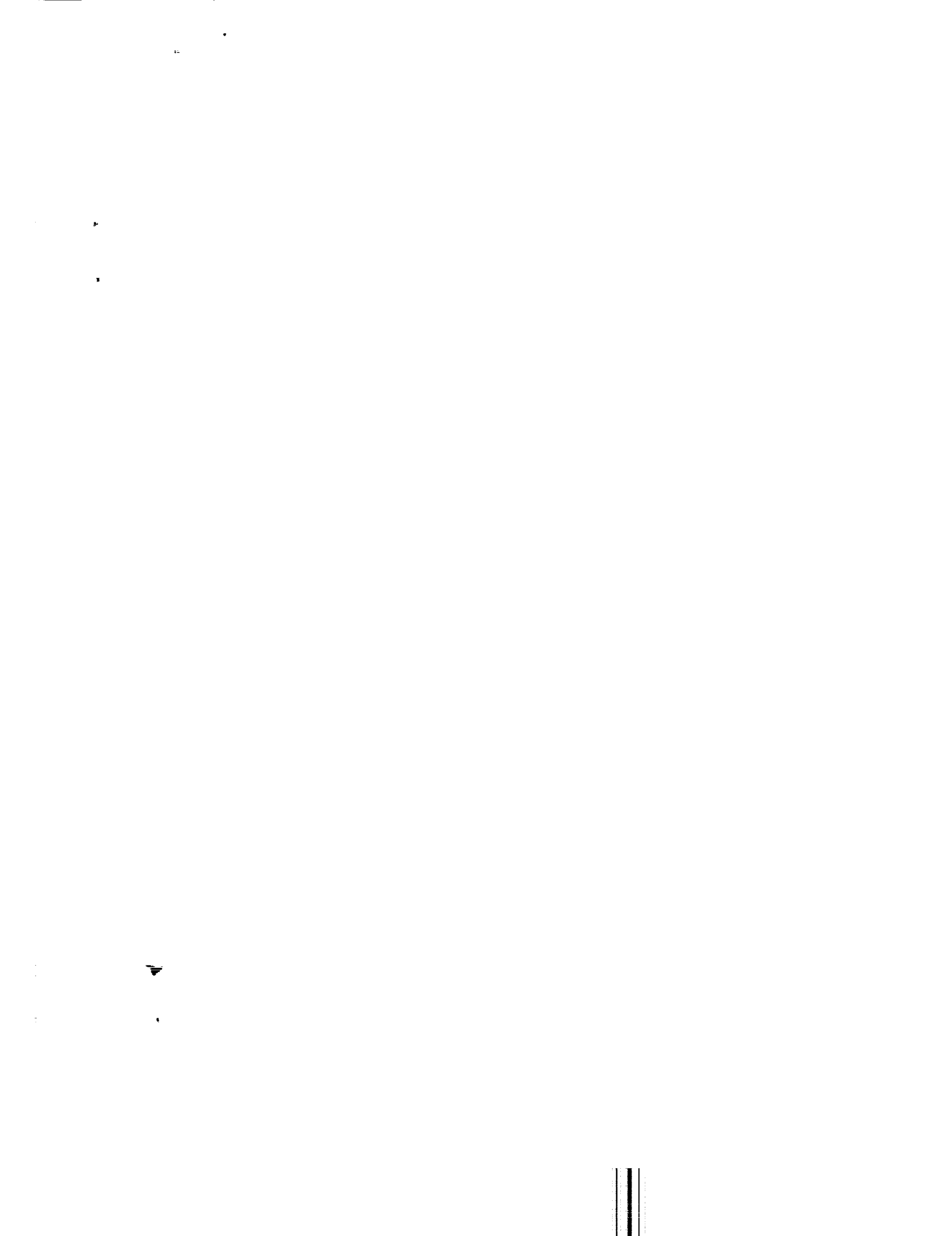
by Marshall C. Burrows and Anatole P. Kurkov

*Lewis Research Center
Cleveland, Ohio 44135*



| | | | |
|--|--|---|---|
| 1. Report No. NASA TM X-2828 | 2. Government Accession No. | 3. Recipient's Catalog No. | |
| 4. Title and Subtitle ANALYTICAL AND EXPERIMENTAL STUDY OF SUPERSONIC COMBUSTION OF HYDROGEN IN A VITIATED AIRSTREAM | | 5. Report Date September 1973 | |
| | | 6. Performing Organization Code | |
| 7. Author(s) Marshall C. Burrows and Anatole P. Kurkov | | 8. Performing Organization Report No. E-6319 | |
| | | 10. Work Unit No. 501-24 | |
| 9. Performing Organization Name and Address Lewis Research Center National Aeronautics and Space Administration Cleveland, Ohio 44135 | | 11. Contract or Grant No. | |
| | | 13. Type of Report and Period Covered Technical Memorandum | |
| 12. Sponsoring Agency Name and Address National Aeronautics and Space Administration Washington, D.C. 20546 | | 14. Sponsoring Agency Code | |
| | | 15. Supplementary Notes | |
| 16. Abstract <p>Detailed probe measurements of total temperature, pressure, and composition were taken in a two-dimensional test section 35.6 cm downstream of hydrogen injection. A high pressure gas generator supplied Mach 2.44 vitiated air or inert gas at elevated temperatures and at a static pressure equal to that of the hydrogen. Special water-cooled probes and sampling techniques were developed for the short test times required by heat-sink hardware. Independent methods of measuring stream total temperatures are compared. For the pure mixing case, the computed composition profile agreed well with the experimental profile. The governing equations were solved numerically by using an implicit finite-difference scheme. The analysis takes into account the wall boundary layer and the initial boundary layer in the main stream. Turbulent shear stress was expressed in terms of an eddy-viscosity model originally developed for turbulent boundary layers. In the case of combustion, results from a combined mixing and equilibrium program were used as a basis for comparison with experimental data. Ignition of hydrogen, as determined from photographic exposures of the radiating gases, varied from 30 to 10 cm downstream from injection for a 45 K increase in local free-stream static temperature.</p> | | | |
| 17. Key Words (Suggested by Author(s)) Reacting flow Supersonic combustion Wall jet Hypersonic propulsion | | 18. Distribution Statement Unclassified - unlimited | |
| 19. Security Classif. (of this report) Unclassified | 20. Security Classif. (of this page) Unclassified | 21. No. of Pages 25 | 22. Price* Domestic, \$2.75 Foreign, \$5.25 |

* For sale by the National Technical Information Service, Springfield, Virginia 22151



ANALYTICAL AND EXPERIMENTAL STUDY OF SUPERSONIC COMBUSTION OF HYDROGEN IN A VITIATED AIRSTREAM

by Marshall C. Burrows and Anatole P. Kurkov

Lewis Research Center

SUMMARY

Detailed probe measurements of total temperature, pressure, and composition were taken in a two-dimensional test section 35.6 centimeter downstream of hydrogen injection. A high pressure gas generator supplied Mach 2.44 vitiated air or inert gas at elevated temperatures and at a static pressure equal to that of the hydrogen. Special water-cooled probes and sampling techniques were developed for the short test times required by heat-sink hardware. Independent methods of measuring stream total temperatures are compared. For the pure mixing case, the computed composition profile agreed well with the experimental profile. The governing equations were solved numerically by using an implicit finite-difference scheme. The analysis takes into account the wall boundary layer and the initial boundary layer in the main stream. Turbulent shear stress was expressed in terms of an eddy-viscosity model originally developed for turbulent boundary layers. In the case of combustion, results from a combined mixing and equilibrium program were used as a basis for comparison with experimental data. Ignition of hydrogen, as determined from photographic exposures of the radiating gases, varied from 30 to 10 centimeters downstream from injection for a 45 K increase in local free-stream static temperature.

INTRODUCTION

The design of supersonic combustors for advanced airbreathing engines requires experimental data on the diffusive mixing and reaction of fuel and air at the high temperatures typical for flight Mach numbers above 6. Reported herein are experimental data analysis for sonic injection of hydrogen from a backward-facing step in a direction parallel to the main supersonic stream.

The mixing of hydrogen with the supersonic airstream has previously been investigated in several different experimental configurations, including parallel or angled flow of hydrogen through slots or arrays of holes (ref. 1). Reacting flows have generally been studied in axisymmetric free-jet or ducted configurations (refs. 2 to 4).

Current techniques of generating a supersonic airstream for combustor testing require an arc heater, storage heater, combustion device, or a combination of the methods. The arc heater and storage heater have the advantage of adding no water vapor to the airstream, but small particulate matter can be entrained in the air from the heater elements. Combustion devices add water vapor, but are generally free of particulate matter.

In the tests reported herein, parallel stepped-wall injection of hydrogen into the combustor was selected for detailed experimental study since it results in minimum disturbance of the free stream when fuel and air pressures are matched. The two-dimensional flow field produced in the test section lends itself readily to studies of ignition delay and mixing lengths, and can be compared with analytical models.

The high temperature gas stream was produced by burning a hydrogen-nitrogen gas mixture with liquid oxygen at high pressure. Each component was regulated so that the desired total temperature was achieved with an oxygen content in the vitiated air stream of about 21 percent by volume. For the nonreacting mixing tests, the gas products contained no oxygen and only a small fraction of hydrogen, similar to the method in reference 3. In this way, it was possible to study the mixing process independently of combustion under approximately the same conditions as that for combustion tests. The balance of products in both cases was composed of nitrogen and water vapor.

The main stream static temperature was generally 1270 K and the static pressure was about atmospheric. The static pressure of hydrogen matched that of the main stream except for ignition tests where hydrogen was preheated to 700 K.

Specially designed probes were constructed to measure total temperature, Pitot and static pressure as well as capture gas samples for mass analysis. A camera recorded onset of combustion through the quartz windows of the test section.

The analysis is based on a numerical solution of boundary layer equations in which the turbulent transport terms were computed by using the concept of eddy-viscosity.

EXPERIMENTAL

Gas Generator

The high-pressure, heat-sink combustion chamber was constructed of electrolytic copper. The internal cross section of the chamber was 5.1 by 9.53 centimeters and its

length was 40.6 centimeters. A 36-element concentric tube injector was used for uniform introduction and mixing of the propellants.

The combustion efficiency, as determined by characteristic exhaust velocity, was approximately 96 percent. The remaining 4 percent was attributed to heat transfer to the inner surfaces of the chamber. A uniform temperature distribution was achieved by inserting two 1.95-centimeter-diameter copper bars at different axial locations in the chamber. Gas generator flows were reproducible within ± 1 percent.

The two-dimensional copper nozzle was designed to supply parallel flow to the test section at Mach 2.44 and atmospheric pressure. Particular care was taken to match the 5.1- by 8.9-centimeter nozzle exit to the test section walls so that no change in area occurred between them. The total temperature profile at the entrance to the test section is shown in figure 1. The values are ratioed to the equilibrium gas temperature calculated from propellant mass flows T_{ref} . The Mach number was within 3 percent of a constant 2.44 in the 6-centimeter core region.

Test Section

The test section (fig. 2) was constructed of four machined copper plates which were bolted together and matched with the nozzle exit. The cross section remained constant to the step. Thereafter, the test section expanded linearly from 5.1 by 9.38 centimeters to 5.1 by 10.5 centimeters at the exit to compensate for boundary layer buildup.

Hydrogen was injected into the test section through the nickel injector parallel to the vitiated air flow at Mach 1 and atmospheric pressure. Lip thickness at the top of the step was 0.076 centimeter. Seven ribs across the 5.1-centimeter width, each 0.076 centimeter thick, straightened the flow and prevented warpage of the top plate and lip. The total temperature of the hydrogen flowing through the slot could be varied from 300 to 800 K. Hydrogen was heated in a storage heater which contained a coil of heavy-walled stainless-steel pipe embedded in a 4.5-kilowatt electric furnace.

Static pressure taps were spaced at 1.25- to 3.8-centimeter increments along the wall downstream from the step and monitored with multiple-scanning pressure transducer. Four 15.1-centimeter-diameter quartz windows were mounted flush with the inner wall surfaces for visual and photographic observations within the test section.

Thermocouple and Pitot Pressure Probes

A water-cooled, wedge-shaped thermocouple probe was designed with a blunted leading edge. The exposed-junction thermocouple could be easily replaced in case of tip failure. Thermocouple materials were iridium - iridium/40 percent rhodium or tungsten - tungsten/26 percent rhenium. Wire diameters ranged from 0.025 to 0.076 centimeter. Temperatures indicated by the thermocouple probe were reproducible with ± 3 percent when care was taken to ensure integrity of wire, junction, and alumina insulator. Readings were taken after junction temperature had stabilized, similar to the procedure in reference 5. A similar water-cooled probe was constructed for Pitot pressure measurements. The pressure port was located in the leading edge of the probe approximately 0.2 centimeter from the end. Pressure measurements were generally within a band of ± 2.5 percent except in the reaction zone, where measurements varied over a wider range from run to run.

In the boundary layer and in the low temperature hydrogen-rich mixing region, miniature swaged thermocouple and miniature Pitot pressure probes were used.

Sampling Probes

Two similar water-cooled probes were designed to obtain gas samples and were also used for indirect temperature measurements. The first probe, designated as Probe I, could be extended into the test section closer to the step. The second probe, designated as Probe II, could only be used in the test section exit plane. The copper cone tip in this probe is replaceable.

The two sampling probe tips are shown in figure 3. In Probe I, water was supplied through circumferentially placed tubes and returned through the annular spaces between the tubes. Water in Probe II was dumped downstream from the tip. Probe I also incorporated three static pressure taps spaced equally around the cone surface 0.635 centimeter downstream from the probe tip.

Both Probes I and II were fitted with a small venturi 15.4 and 11.8 centimeters downstream, respectively. Each venturi was instrumented with two pressure taps and a small thermocouple. A second venturi was placed downstream between the probe sample outlet and the sample container, and was also equipped with pressure taps and a thermocouple. Analysis of the trapped samples was done on a mass spectrometer, and on a dry basis, was accurate within 2 percent. The amount of water vapor in each trapped sample was deduced from the difference in the hot and cooled gas mass flows, after adjusting for saturated gas flow in the second venturi. The water droplets which collected on the inner wall of the sample line were purged out with helium before each

succeeding run. Calculated compositions were generally within ± 2 percent of faired curves drawn through the data points.

In calculating the mass flow through the probe venturi, it was assumed that the gas bulk temperature T_1 is related to the measured thermocouple temperature T_m according to the following relation:

$$T_1 = T_m \left[1 - \frac{0.21(T_m - T_w)}{T_m} \right] \quad (1)$$

where T_w is the tube wall temperature which is taken to be equal to the cooling water temperature. This follows from the velocity profile given in reference 6 and the assumption that the velocity and temperature profiles are similar. A similar conclusion is also reached from the data presented in reference 7.

The transport properties of the gaseous mixture, which are necessary for the determination of the Reynolds and Prandtl numbers, were calculated using approximate relations essentially identical to those presented in reference 8. Collision cross section data were obtained from R. Svehla of NASA Lewis Research Center.

The sampling probes were calibrated with reference flow nozzles over a range of flows corresponding to the Reynolds number range encountered in the test runs. Heat transfer characteristics of each probe were obtained using heated nitrogen.

The sampling probes were also used as cooled-gas pyrometers to indirectly measure the stream total temperature, as done in reference 9.

Procedure

Runs were sequenced for 3 seconds duration with steady-state flows established for 2.5 seconds or longer. Motion picture analysis verified stability of the combustion process above the ignition limits. Generally, all readings were taken 2.5 seconds after initiation of each run. Instrumentation probes used in the test section were moved incrementally between succeeding runs to obtain the profiles of Pitot pressure, total temperature, and composition.

Sampling probe cooling water was preheated nearly to the boiling point to prevent condensation within the probe. A helium purge through the probe prevented composition errors due to residual gases. During normal operations, the helium was swept out of the lines during the run and replaced by sample gases.

Static pressures were measured at the entrance to the test section, along the wall downstream from the hydrogen injection step, in the gas generator, and upstream from the sonic-flow nozzles in the nitrogen and hydrogen supply lines.

ANALYSIS

The governing equations considered in the analysis are time-average, boundary-layer equations for conservation of mass, momentum, and energy. The mass conservation equations include the overall continuity equation and the specie conservation equations. The turbulent shear stress terms were introduced using the concept of eddy viscosity, and turbulent Prandtl and Lewis numbers were assumed to equal unity.

The solution was obtained in streamline coordinates by using an implicit-finite difference method. The procedure follows a more general method described in reference 10. The simplification in this case results from the assumption of a uniform pressure field normal to the streamlines. Therefore, the second momentum equation becomes superfluous. This is justified because in the experiment there was no appreciable difference in the static pressures between the main stream and the hydrogen jet, and there was no evidence of significant pressure change in the transverse direction in the downstream region.

The initial velocity and temperature profiles (fig. 4) were obtained from measurements just downstream of the injector. On the hydrogen side the flow was assumed to be uniform because the Pitot probe size (0.81 mm) was too large to measure the true profile. Since no initial composition measurements were taken, the initial composition profile has been taken to correspond to the step distribution.

In the actual computation for the pure mixing case, the slight change in the free stream properties from the injection point to the exit of the test section encountered in the experiment has been neglected. Final free stream properties were assumed in the initial profiles. For the combustion case, however, a linear change in free stream properties throughout the test section has been assumed, so that initial and final free stream properties correspond to experimental values.

The boundary conditions at the wall are: zero velocity for the momentum equation, constant temperature $T = 298 \text{ K}$ for the energy equation, and zero slope for the specie conservation equation. The constant-temperature boundary condition is a good approximation, because of the short duration runs used in the experiment, and the good heat-sink capacity of the wall.

The basic assumption in the viscosity formulation is that it is related to the viscosity in the turbulent boundary layer. This appears to be justified, because the initial velocity profile is essentially the result of the main-stream boundary layer, and because in the far region, the boundary layer on the wall merges with the mixing region, and the velocity distribution approaches again the turbulent boundary-layer profile.

The boundary-layer effective-viscosity hypothesis assumed in the analysis is due to Mellor (ref. 11). The details of formulation may be found in reference 12 where the

viscosity hypothesis was extended for compressible flow. The molecular viscosity, which is needed in the analysis, was determined using the relations presented in reference 8.

Figure 5 illustrates the velocity profile in the region where the wall boundary layer is still developing independently of the mixing region.

Between points 1 and 2 viscosity is determined according to the turbulent boundary-layer effective-viscosity hypothesis. Between points 2 and 3 it is very small, approaching the molecular viscosity, and between points 3 and 4 it is determined as in the outer portion of the boundary layer. Points 2 and 3 were chosen so that the deviation from uniform flow is about 0.1 percent. When points 2 and 3 merge farther downstream, the region is treated as a turbulent boundary layer.

In order to be able to resolve the laminar sublayer region next to the wall without using an excessive number of points normal to the streamlines, it was necessary to use variable mesh spacing.

At present, combustion reactions are incorporated in the analysis by assuming chemical equilibrium. Despite its inherent limitations, this assumption is useful in that it provides a basis for comparison for the experimental data. The departure of experimental results from the equilibrium solution underlines the nonequilibrium effects.

The formulation of chemical equilibrium equations is as in reference 13. In addition to stable species (hydrogen, oxygen, nitrogen, and water), atomic hydrogen, atomic oxygen, and hydroxyl radical were assumed to be present. In the low temperature region the thin flame solution as formulated in reference 14 has been used.

The mixing model was assumed to be unaltered by the reaction, and in the equilibrium calculation time-average properties were used.

RESULTS AND DISCUSSION

Experimental Profiles

Measurements. - Composition, Pitot pressure, and total temperature in the combustion region were obtained for free stream conditions at the entrance to the test section of Mach 2.44, atmospheric pressure, and for static temperatures generally in the range 1250 to 1270 K. In the pure mixing case, the Mach number and static pressure were about the same while the static temperature was slightly lower, or about 1150 K. In both cases, hydrogen was injected at sonic velocity, matched static pressure, and a total temperature which was slightly above ambient temperature in most .

cases. These input conditions will be assumed to apply to the data unless other conditions are specifically stated.

The majority of results were obtained at the test section exit plane 35.6 centimeters downstream from the hydrogen injection step. Hence, in reporting the results, this station will be implied unless otherwise noted. The thermocouple probe and Pitot pressure probe were retracted slightly from the test section exit plane to ensure that the detached shock off the probe leading edge does not extend inside the test section.

Composition. - The composition profile for the reacting case is shown in figure 6. The measured free stream composition matches the theoretical composition obtained from gas generator performance calculations. Water vapor volume fraction is maximum at about 2.2 centimeters, and the mixing boundary extends approximately to 2.9 centimeters from the stepped wall. Total spreading angle of hydrogen away from the wall is 3.9° . Both oxygen and hydrogen are present in small amounts in a narrow region around $Y = 2.2$ centimeters. Composition variations during the run or partial quenching of the chemical reactions can account for this. A similar result was noted in reference 2.

A small volume fraction of oxygen is present in the hydrogen-rich region near the stepped wall. Apparently, diffusion of oxygen into the hydrogen took place in the region between the step and the point where the flame is initiated.

The composition profile for the nonreacting case is presented in figure 7. In this case gas samples were taken by using the Pitot pressure probe, and consequently, measurements of the sample water content were not made. It was assumed that the ratio of volume fractions of water vapor and nitrogen is constant. The mixing boundary extends about 2.3 centimeters from the stepped wall, resulting in a spreading angle for hydrogen of 2.9° .

Pitot pressure. - The Pitot pressure measurements are presented in figure 8. The reference pressure noted in this figure was taken to be equal to the gas generator pressure. In this way, run-to-run variations in Pitot pressure due to slight changes in propellant flows are reduced. The initial boundary layer thickness is about 1 centimeter while the width of the disturbed region is about 2.4 centimeters for the pure mixing case, and about 3.1 centimeters for the reacting case. These values are close to the boundaries determined from the composition profiles. Pitot pressures in the combustion region varied considerably during the run, indicating some fluctuation in the combustion process.

Temperature. - Most of the measurements were made using iridium - iridium/40 percent rhodium bare wire thermocouples and are shown in figure 9. The radiation correction was made according to the equations presented in references 15 and 16. The emissivity of the iridium and the iridium-rhodium alloy was assumed equal to the emissivity of platinum (ref. 17). The emissivity data were obtained from reference 18.

The recovery correction was estimated from the results obtained for similar type thermocouples in references 19 and 20. The radiation correction did not exceed 85 K, while the maximum recovery correction was about 70 K.

The points close to the stepped wall for $X = 0$ and $X = 18.3$ centimeters and the two points at $X = 33$ centimeters were obtained using miniature thermocouples. The tailed symbol for $Y = 1.9$ centimeters at the test section exit was obtained using a tungsten - tungsten/26 percent rhenium thermocouple. It should be noted that the indicated temperature for this point could be in error because of oxidation of the thermocouple surface. However, examination of gas composition in figure 6 indicates that only a small amount of oxygen is likely to be present at this position. It is also noted that at a somewhat lower free stream temperature, for the position of $Y = 1.59$ centimeters, the temperature obtained with a tungsten-rhenium alloy thermocouple agreed well with the value obtained at the same position using an iridium-rhodium alloy thermocouple.

The location of the maximum temperature in the combustion case at $Y = 1.9$ centimeters is closer to the stepped wall than the location of the maximum water volume-fraction shown in figure 6.

The reference temperature, used to ratio the values of total temperature in figure 9, is the calculated gas generator temperature for each particular run. Its representative average value is noted in the legend.

The total temperature was also calculated from the measurement of the gas sample temperature at the probe venturi using Probes I and II as cooled-gas pyrometers, according to the method outlined in reference 9.

The cooled-gas bulk temperature T_1 is related to the total temperature at the probe entrance T_0 by the following equation:

$$T_0 = (T_1 - T_w) \exp \left[\left(\frac{4X_t}{d} \right) St \right] + T_w \quad (2)$$

where T_w is the average tube wall temperature and is assumed equal to the average water temperature; X_t is the probe thermocouple location measured from the probe tip; d is the inside diameter of the tube; and St is the Stanton number.

The Stanton number is given as a function of Reynolds number Re and Prandtl number Pr by the following relation (refs. 18 and 21):

$$St = H_c Re^{-a} Pr^{-0.667} \quad (3)$$

where H_c and a are constants which are determined by calibration. The Prandtl number and the viscosity in the Reynolds number were calculated for an average film temperature T_f which was given by the equation

$$T_f = \frac{\frac{(T_1 + T_0)}{2} + T_w}{2} \quad (4)$$

Probes I and II were calibrated using the total temperatures obtained from direct thermocouple probe measurements in the test section and using the data obtained in a special calibration using preheated nitrogen. The results for Probe I showed $H_c = 0.0255$ throughout the range of flows. The results for Probe II are shown in figure 10. The points which fell above the $H_c = 0.067$ line in the low Reynolds number region were all taken for small values of Y , where it is believed that the thermocouple temperatures were in error because of the boundary layer separation induced by the thermocouple probe. This is substantiated in figure 9, where two points at $X = 33$ centimeters taken with a miniature thermocouple fell considerably below the points at the 35.6-centimeter measuring station.

The tailed symbols in figure 10 deviate markedly from the $H_c = 0.067$ line. They fall just to the left and to the right of the maximum temperature region. (The measured temperature using the tungsten-rhenium alloy thermocouple was not included.) One reason for the deviation in H_c may be due to the different flow regime in this low Reynolds number and high temperature region. In this case there is some justification for assuming a local calibration line $H_c = 0.055$ for the positions which lie between the tailed symbols. There is less justification for this assumption if the deviation of H_c is due to chemical reactions within the probe. However, if the aforementioned two values of H_c are used to calculate the total temperatures, the results are as shown in figure 11. Also included in this figure are temperatures which were computed from measurements made using Probe I, which had a constant value of H_c .

For the purpose of comparison, figure 11 also includes curves reproduced from figure 9. The dashed line close to the stepped wall passes through the cooled-gas pyrometer points. It also coincides with the two points measured with the miniature thermocouple at the $X = 33$ -centimeter station (fig. 9). In general, a fair agreement is noted for total temperatures derived by two different methods. The cooled-gas pyrometer using Probe I gives somewhat higher values in the reaction region for the hydrogen-vitiated air case and in a portion of the mixing region for the pure mixing case.

Flow field. - The complete flow field at the test section exit plane was first calculated assuming that static pressure was uniform and equal to the wall static pressure

at the 33-centimeter station. The composition was assumed given by the curves in figures 6 and 7 while the total temperature and Pitot pressure were obtained from faired curves in figures 11 and 8, respectively. The static pressure on the cone surface was then calculated for the positions indicated in table I and compared with the measured cone static values. This iterative procedure on stream static pressure was repeated until calculated and measured values of cone static pressures agreed. Table I lists the final values of static pressure in the free stream region. For final computation of the flow field, the static pressure value in the right column of table I was used as a representative value for each test.

The cone flow solution described previously was obtained for the hollow cone geometry of Probe I by using rotational characteristics theory. Caloric imperfections have been included in the calculations.

Comparison with Analysis

Composition. - For the pure mixing case, good agreement with the experiment was obtained without any adjustment of constants in the turbulent transport model. In fact, the computed curves shown in figure 7 were also used as faired curves for the experimental points.

In the case of combustion, experimental results were compared with analysis based on chemical equilibrium (fig. 12). Physically, this situation corresponds to the case when the main stream static temperature is high, so that ignition delay and reaction times are small in comparison with the flow time. Although in the experiment the ignition delay was not negligible, there appears to be a fair degree of similarity between the computed and experimental composition profiles. The main difference is that the experimental profiles appear to be shifted away from the wall. This could be explained by the fact that in the experiment the rate of reaction depends strongly on temperature, and hence, ignition occurs in the lean mixture region, where the static temperature is high. The equilibrium assumption in the calculation, however, causes the peak in water vapor and related consumption of reactants to occur near the stoichiometric plane, which also corresponds to the maximum temperature plane.

The displacement of the two sets of composition profiles could also be attributed to perhaps a higher effective viscosity in the flame region. However, in order to effect such a displacement in the computed profiles, the viscosity would have to be considerably increased in the region around the reaction zone. As a consequence, the slopes of the computed profiles would become much more gradual, and produce unacceptable profile shapes.

It can be seen from the experimental profiles in figure 12 that in a narrow region around $Y = 2.2$ centimeters both oxygen and hydrogen are present in small amounts. This could either be due to the composition variation during the run or due to the partial quenching of the chemical reactions. It can be seen that the concentration of reactants is higher in this region, and that the width of the region is greater than in the case of equilibrium.

Total temperature and Mach number. - In figures 13 and 14 comparison is made between computed and experimental total temperature and Mach number profiles for both mixing and combustion cases. From the results for pure mixing it may be concluded that in the experiment there was excessive flow deceleration near the wall. It is believed that this is caused by boundary layer buildup in the corners of the test section. This effect strongly influences only the velocity and temperature fields. The concentration field is largely independent of it, however, because the boundary condition at the wall is different in this case.

The maximum of the experimental total-temperature profile in figure 13 is 91 percent of the corresponding point in the computed profile. This, again, indicates the extent of departure from equilibrium in the experiment.

The reduction in Mach numbers for combustion case in comparison with the pure mixing case is evident in figure 14. The effect is similar in both computed and experimental profiles and is a result of heat addition.

Ignition Characteristics

Ignition delays were determined from photographs of OH radiation which originated at various distances downstream from hydrogen injection. Results of these measurements are shown in figure 15 as a function of local free stream static temperature. Since the free stream static temperature gradually increased with axial distance, the value at each data point was linearly interpolated between entrance and exit static temperatures. Distances required for ignition increased linearly with a slight decrease in local static temperature, but did not change for a 400 K increase in total hydrogen temperature. Hydrogen flow was the same in both cases.

Combustion within the test section could also be detected by measurement of wall static pressures. The static pressure distribution for mixing and combustion cases is shown in figure 16. There is evidence of a slight expansion at $X = 2$ centimeters and a subsequent recompression near $X = 8$ centimeters in both profiles. The static pressure rise at 18 centimeters is attributed to combustion initiation and agrees reasonably well with the onset of ultraviolet radiation. For a range of ignition distances, static

pressure rise was not a reliable indication of reaction, especially at lower temperatures.

The ignition distances in figure 15 can be used to estimate induction times and compare them with analytical and published results. Since a 400 K change in total temperature of hydrogen did not affect the ignition limits, it was assumed that ignition originated in a lean mixture range in a region close to the free stream. Experimental induction times ranged from 69×10^{-6} to 207×10^{-6} second for the values of local free stream static temperature between 1305 and 1260 K, velocity of 1600 meters per second, and ignition distance variation from 10 to 30 centimeters.

Induction times reported in reference 22 for lean hydrogen-oxygen mixtures at the temperature of 1265 K varied from 69×10^{-6} to 333×10^{-6} second for H_2/O_2 ratios between 0.064 and 0.0075, respectively. From this agreement, it may be concluded that it is possible for ignition to occur in a lean H_2 -vitiated air range where hydrogen volume fraction is less than 0.0133.

A one-dimensional kinetics program by Bittker and Scullin (ref. 23) can also be used to obtain results for comparison with the experimental data. If an H_2/O_2 ratio of 0.013, temperature of 1270 K, and free stream mixture of N_2 , O_2 , H_2O , and NO were assumed in the test section, an induction time of 90×10^{-6} second was determined. Induction time was defined as the intercept of the maximum slope of the temperature-time curve with the 1270 K line. A decrease in the assumed mole fraction of NO increased the induction time. However, if the one-dimensional program is initiated in the gas generator with initial reactants, calculated species in the test section include radicals such as OH , with a mole fraction of 3.4×10^{-4} . This high radical concentration effectively reduces the induction period for the same lean mixtures to 8×10^{-6} second or less.

In the experiment, the OH radicals may be destroyed in the boundary layer region because of lower local temperatures and wall effects. Therefore, for a better agreement with the experiment, it appears that two-dimensional effects need be incorporated in the ignition delay calculations.

CONCLUDING REMARKS

With regard to experimental techniques, the following results have been demonstrated:

1. Adequate reproducibility of test runs can be obtained using the reported techniques for production of vitiated air and acquisition of data, so that short duration runs - sufficient to record data at one position only - can be employed in conjunction with heat sink hardware.

2. Several simultaneous measurements can be combined in a single sampling probe. Total temperature is deduced from the cooled-gas temperature; water vapor content of sample is determined from the difference between hot and cold gas flows; and static pressure is deduced from the measurements of pressure on the surface of the open-core tip of the probe.

The following statements can be made with regard to experimental results and their comparison with analysis:

1. Experimental mixing zone boundaries based on 1 percent deviation from the free stream volume fraction of water vapor are somewhat wider in the reacting case compared with pure mixing case.

2. For the pure mixing case, the composition field can be predicted by using an effective viscosity which is based on hypothesis originally developed for turbulent boundary layers.

3. Comparison of experimental data for combustion case with theory based on chemical equilibrium indicates that: (a) the maximum total temperature obtained in the experiment is 91 percent of the theoretical value; (b) both reactants, hydrogen and oxygen, are simultaneously present in larger amounts and over a wider region than determined by theory; and (c) the center of the reaction zone in the experiment is positioned further out in the free stream. All of these effects are believed to be due to finite-rate chemistry.

4. Ignition of hydrogen within the test section was dependent on free stream temperature but unaffected by a 400 K increase in hydrogen temperature. Apparently ignition originated in fuel-lean mixtures close to free stream temperature. Measured induction times were considerably longer than those predicted by a one-dimensional kinetic calculation which includes the effect of free stream radicals produced in the gas generator. However they agreed with values reported in the literature for lean mixtures in a shock tube which contained no free radicals. This discrepancy indicates a need to incorporate two-dimensional effects in the calculation.

In general, the results of this study show that parallel wall injection of hydrogen in a practical configuration is dominated by the boundary layer phenomenon. Total spreading angle of hydrogen away from the wall, which would be useful for design purposes, is 3.9° in the reacting case and 2.9° in the mixing case. The relatively slow rate of depletion of hydrogen near the wall also suggests the use of this injection method to provide film cooling to combustor walls.

Lewis Research Center,

National Aeronautics and Space Administration,

Cleveland, Ohio, June 26, 1973,

501-24.

REFERENCES

1. Schetz, J. A.; Gilreath, H. E.; and Lubard, S. C.: Fuel Injection Mixing in a Supersonic Stream. Twelfth Symposium (International) on Combustion. Combustion Institute, 1969, pp. 1141-1149.
2. Anderson, Griffin Y.; Agnone, Anthony M.; and Russin, Wm. Roger: Composition Distribution and Equivalent Body Shape for a Reacting, Coaxial, Supersonic Hydrogen-Air flow. NASA TN D-6123, 1971.
3. Cohen, Leonard S.; and Guile, Roy N.: Measurements in Free Jet Mixing/ Combustion Flows. Paper 69-538, AIAA, June 1969.
4. Billig, F. S.; and Dugger, G. L.: The Interaction of Shock Waves and Heat Addition in the Design of Supersonic Combustor. Twelfth Symposium (International) on Combustion. Combustion Institute, 1969, pp. 1125-1139.
5. Burrows, Marshall C.: Thermometric Determination of Oxidant-Fuel Distribution Within a Rocket Combustor. NASA TN D-5626, 1970.
6. Schlichting, Hermann (J. Kestin, trans.): Boundary Layer Theory. McGraw-Hill Book Co., Inc., 1955, pp. 502-508.
7. Eckert, E. R. G.; and Drake, Robert M., Jr.: Introduction to the Transfer of Heat and Mass. McGraw-Hill Book Co., Inc., 1950, p. 125.
8. Brokaw, Richard S.: Alignment Charts for Transport Properties Viscosity, Thermal Conductivity, and Diffusion Coefficients for Nonpolar Gases and Gas Mixtures at Low Density. NASA TR R-81, 1961.
9. Krause, Lloyd N.; Johnson, Robert C.; and Glawe, George E.: A Cooled-Gas Pyrometer for Use in High-Temperature Gas Streams. NACA TN 4383, 1958.
10. Kurkov, Anatole P.: Mixing of Supersonic Jets Including the Effects of Transverse Pressure Gradient Using Difference Methods. NASA TN D-6592, 1971.
11. Mellor, G. L.; and Gibson, D. M.: Equilibrium Turbulent Boundary Layers. J. Fluid Mech., vol. 24, pt. 2, Feb. 1966, pp. 225-253.
12. Herring, H. James; and Mellor, George L.: A Method of Calculating Compressible Turbulent Boundary Layers. NASA CR-1144, 1968.
13. Hopf, H.; and Fortune, O.: Diffusion Controlled Combustion for Scramjet Applications Part II, Programmer's Manual. Tech. Rep. 569, General Applied Science Lab., Inc., 1965.
14. Da-Riva, I.: The Internal Structure of Hydrogen-Air Diffusion Flames. *Astronautica Acta*, vol. 12, no. 4, 1966, pp. 284-293.

15. Scadron, M. D.; Warshawsky, I.; and Gettelman, C. C.: Thermocouples for Jet-Engine Gas Temperature Measurements. ISA Proc. vol. 7, 1952, pp. 142-148.
16. Glawe, George E.; Simmons, Frederick S.; and Stickney, Truman M.: Radiation and Recovery Corrections and Time Constants of Several Chromel-Alumel Thermocouple Probes in High-Temperature, High-Velocity Gas Streams. NACA TN 3766, 1956.
17. Glawe, G. E.; Johnson, R. C.; and Krause, L. N.: Intercomparison of Several Pyrometers in a High-Temperature Gas Stream. Temperature - Its Measurement and Control in Science and Industry. Vol. 3, Part 2. Reinhold Publ. Co., 1962, pp. 601-605.
18. McAdams, William H.: Heat Transmission. Third ed., McGraw-Hill Book Co., Inc., 1954.
19. Simmons, Frederick S.: Recovery Corrections for Butt-Welded, Straight-Wire Thermocouples in High-Velocity, High-Temperature Gas Streams. NACA RM E54G22a, 1954.
20. Stickney, Truman M.: Recovery and Time-Response Characteristics of Six Thermocouple Probes in Subsonic and Supersonic Flow. NACA TN 3455, 1955.
21. Kreith, Frank: Principles of Heat Transfer. International Textbook Co., 1958, pp. 346-347.
22. White, D. R.; and Moore, G. E.: Structure of Gaseous Detonation. IV. Induction Zone Studies in H_2-O_2 and $CO-O_2$ Mixtures. Tenth Symposium (International) on Combustion. Combustion Institute, 1965, pp. 785-795.
23. Bittker, David A.; and Scullin, Vincent J.: General Chemical Kinetics Computer Program for Static and Flow Reactions, With Application to Combustion and Shock-Tube Kinetics. NASA TN D-6586, 1972.

TABLE I. - STATIC PRESSURE IN

FREE STREAM REGION

| Case | Probe position, cm | Static pressure, N/m ² | |
|----------|--------------------|-----------------------------------|----------------------|
| | | Local | Assumed |
| Reacting | 3.81 | 1.21×10 ⁵ | 1.17×10 ⁵ |
| | 3.18 | 1.19 | 1.17 |
| | 2.54 | 1.16 | 1.17 |
| Mixing | 5.08 | 1.10×10 ⁵ | 1.10×10 ⁵ |
| | 3.81 | 1.13 | 1.10 |
| | 3.18 | 1.12 | 1.10 |

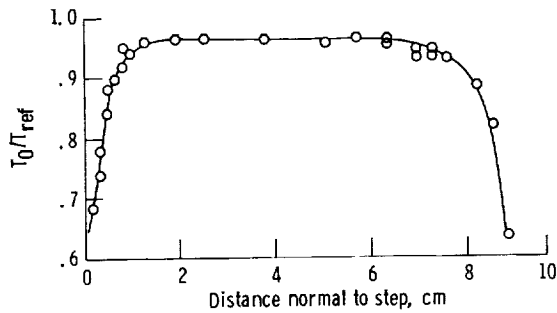


Figure 1. - Total temperature ratio at injection step; vitiated air.

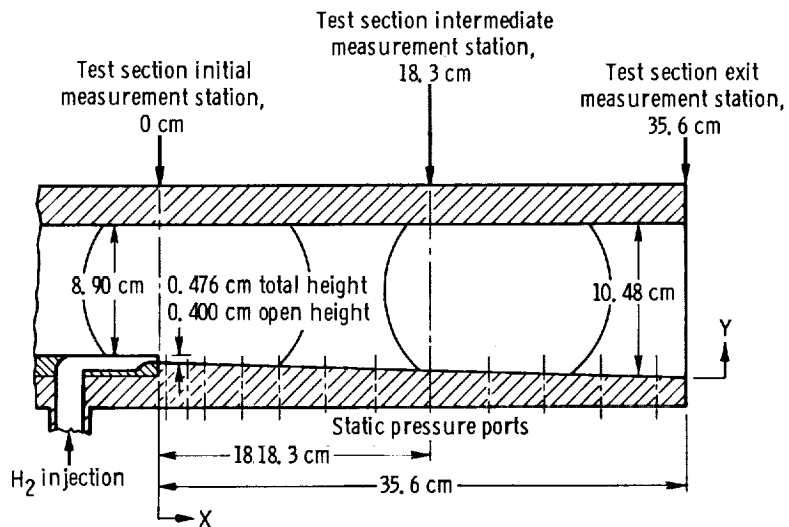
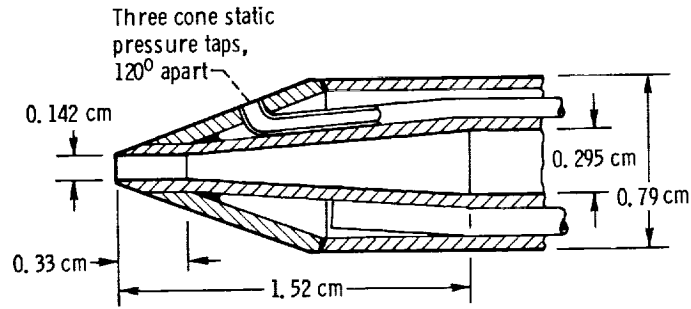
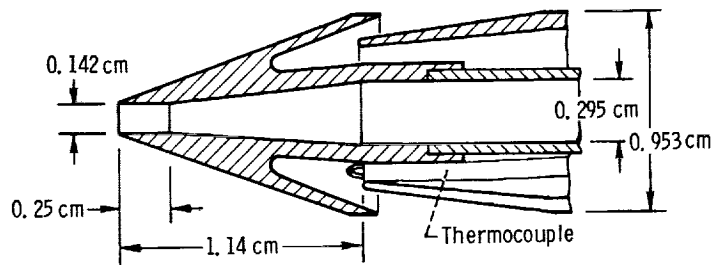


Figure 2. - Test section showing hydrogen injection step, location of static pressure ports, and measurement stations.



(a) Probe I tip design; closed circuit cold water cooling at $5.34 \times 10^6 \text{ N/m}^2$ pressure.



(b) Probe II tip design; open circuit hot water cooling at $1.72 \times 10^6 \text{ N/m}^2$ pressure.

Figure 3. - Sampling probe tip details.

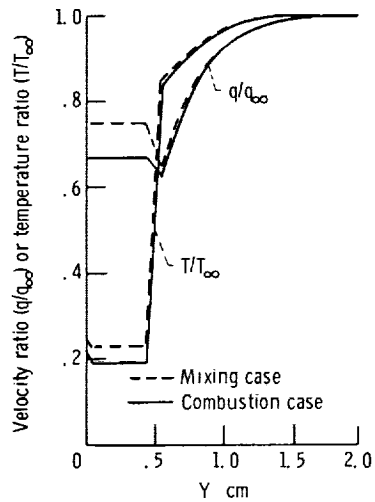


Figure 4. - Initial velocity and temperature profiles at injection step.

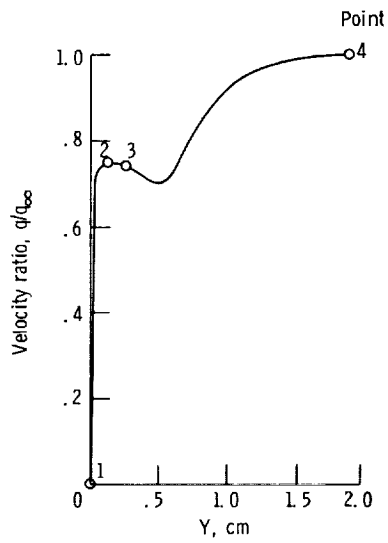


Figure 5. - Intermediate velocity profile.

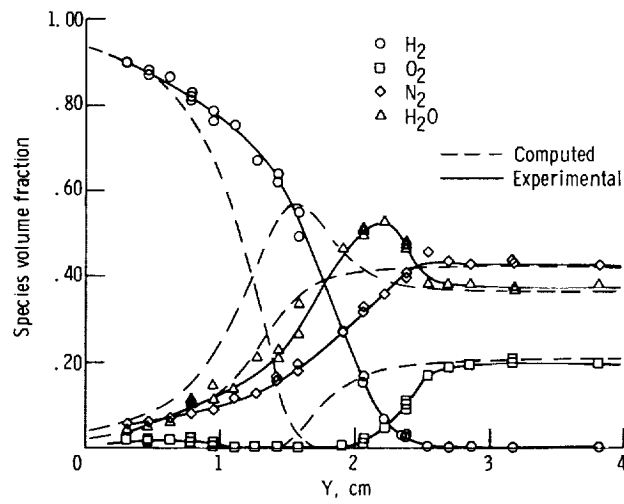


Figure 6. - Composition profile using Probe II. $X = 35.6$ centimeters; hydrogen-vitiated air. Calculated composition of vitiated air, $H_2 = 0$, $O_2 = 0.203$, $N_2 = 0.438$, $H_2O = 0.359$.

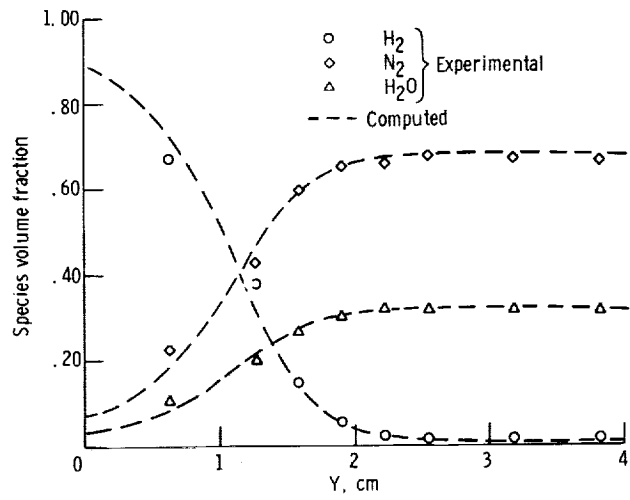


Figure 7. - Composition profile for mixing case $X = 35.6$ centimeters; hydrogen-inert gas.

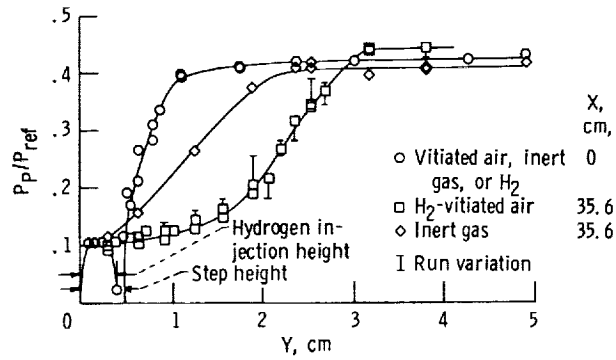


Figure 8. - Pitot pressure profiles. Vitiated air, $P_{ref} = 17.1 \times 10^5$ N/m²; inert gas, $P_{ref} = 18.5 \times 10^5$ N/m².

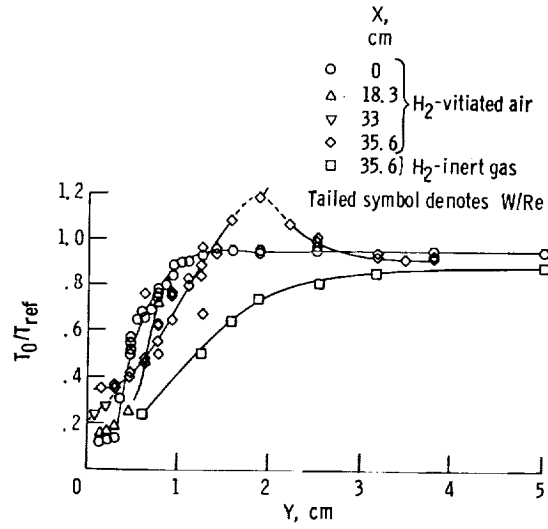
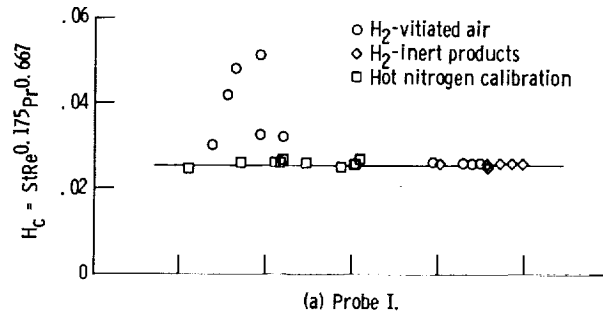
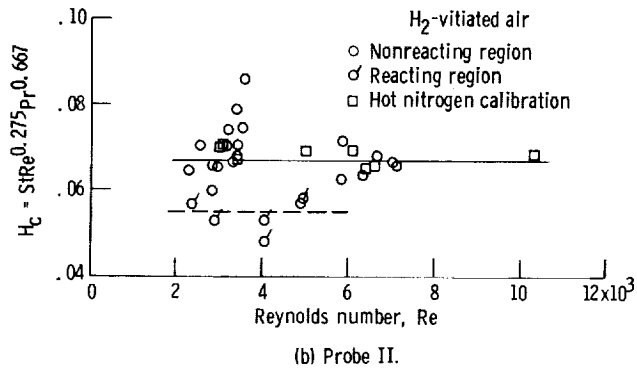


Figure 9. - Total temperature ratios from thermocouple measurements. Vitiated air, $T_{ref} = 2380$ K; inert gas, $T_{ref} = 2276$ K.



(a) Probe I.



(b) Probe II.

Figure 10. - Heat transfer calibrations.

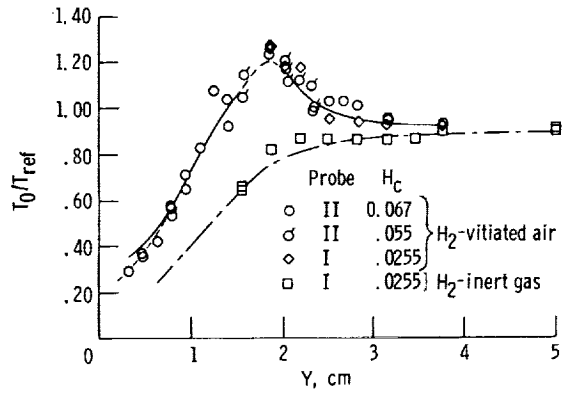


Figure 11. - Total temperature ratio from cooled-gas pyrometer measurements. $X = 35.6$ centimeters; vitiated air, $T_{ref} = 2380$ K; inert gas, $T_{ref} = 2276$ K.

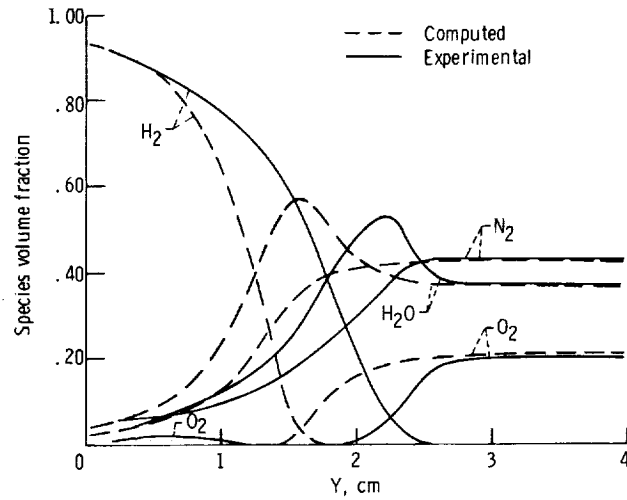


Figure 12. - Computed and experimental composition profiles combustion case.

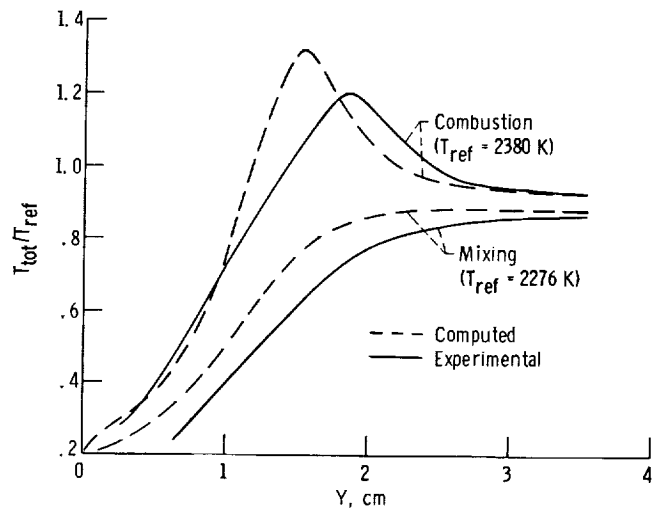


Figure 13. - Total temperature profiles.

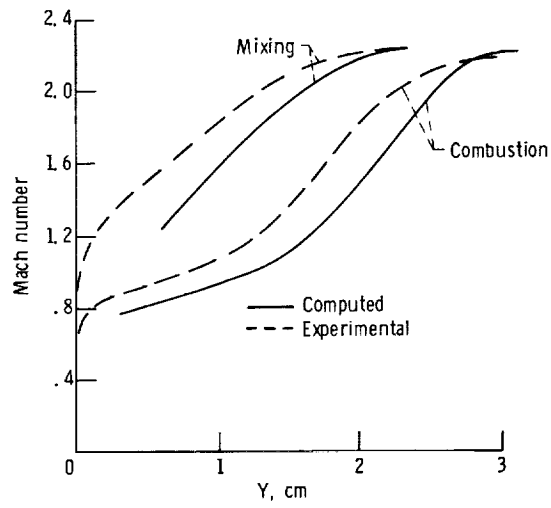


Figure 14. - Mach number profiles.

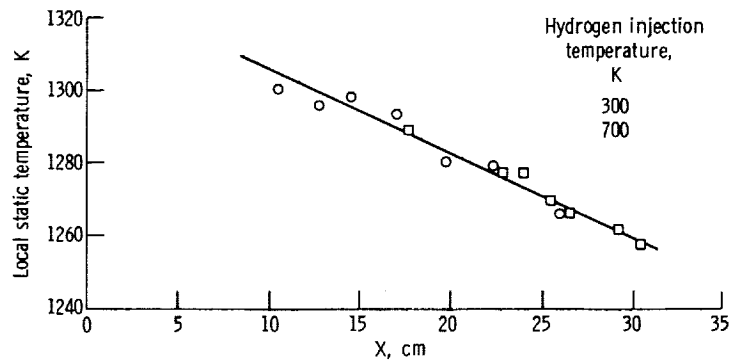


Figure 15. - Hydrogen-vitiated air ignition distances determined by onset of ultraviolet radiation.

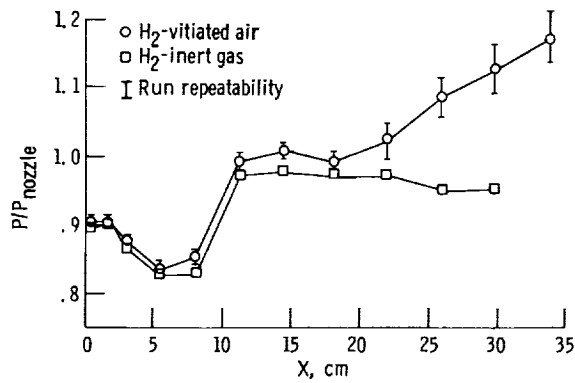


Figure 16. - Wall static pressure ratio. $P_{\text{nozzle}} = 0.917 \times 10^5 \text{ N/m}^2$.





